Li distribution characterization in Li-ion batteries positive electrodes containing $Li_xNi_{0.8}Co_{0.15}Al_{0.05}O_2$ secondary particles ($0.75 \leqslant x \leqslant 1.0$)

K. Mima , R. Gonzalez-Arrabal , H. Azuma , A. Yamazaki , C. Okuda , Y. Ukyo , H. Sawada , K. Fujita , Y. Kato , J.M. Perlado , S. Nakai

A B S T R A C T

The elemental distribution of as-received (non-charged) and charged Li-ion battery positive electrodes containing $Li_xNi_{0.8}Co_{0.15}Al_{0.05}O_2$ ($0.75 \leqslant x \leqslant 1.0$) microparticles as active material is characterized by combining μ-PIXE and μ-PIGE techniques. PIGE measurements evidence that the Li distribution is inhomogeneous (existence of Li-rich and Li-depleted regions) in as-received electrodes corresponding with the distribution of secondary particles but it is homogeneous within the studied individual secondary micro-particles. The dependence of the Li distribution on electrode thickness and on charging conditions is characterized by measuring the Li distribution maps in specifically fabricated cross-sectional samples. These data show that decreasing the electrode thickness down to 35 μm and charging the batteries at slow rate give rise to more homogeneous Li depth profiles.

1. Introduction

The development of efficient storage technologies for electrical energy plays an important role mainly in the progress of portable consumer electronics and electric vehicles. Nowadays, Li-ion batteries are attractive candidates for these applications since they can provide high energy and high power densities. The performance of a Li-ion battery is mainly governed by its energy density, power, capacity, charge and discharge rates as well as, its lifetime.

Basically, Li-ion batteries consist of a positive and a negative electrode separated by an electrolyte layer, which must be an ionic conductor and electronic insulator. Once positive and negative electrodes are linked by an external circuit, spontaneous electrochemical reactions take place, in which chemical energy is transformed into electrical energy, namely, the discharge process takes place. For the reverse reaction, an electric current has to be applied. These reactions involve the lithium-ion diffusion between the positive and the negative electrodes [1]. Therefore, the performance of a Li-ion battery strongly depends, among other factors, on the characteristic of the electrodes and in particular on the Li-ion diffusion capabilities on it. Because of this reason the study of the Li distribution in the positive electrode is one of the main points of concern in further battery development.

However, Li characterization is not a trivial task, in particular, if depth resolution is required. The Li distribution in regions close to the sample surface can be inferred from electron spectroscopy techniques [2–4]. However, the basics of these techniques hamper to carry out precise Li distribution characterization mainly because of two reasons: (i) the total amount of Li cannot be accurately characterized, (ii) as a result of electron-matter interaction they can only be used for characterization in the near surface region with low spatial resolution. Some other material analysis methods such as laser induced breakdown spectroscopy or atomic absorption have also poor sensitivity to measure the Li concentration. Synchrotron Radiation (SR) has been also applied to characterize Li distribution by measuring the absorption edge shift of Co, Ni, and so on, using the X-ray absorption fine structure techniques (XAFS), although the Li determination measurement is indirect [5,6].

Ion beam analysis (IBA) techniques [7] are powerful tools which permit direct, nondestructive and accurate quantitative elemental concentration characterization, including light ions such as Li [8,9]. Moreover, the use of μ-beam scanning procedures allows studying elemental concentration distributions with high lateral resolution (in the μm range).

In this paper we investigate the Li and Ni distribution for as-received and charged positive electrode containing $Li_xNi_{0.8}Co_{0.15}Al_{0.05}O_2$ ($0.75 \leqslant x \leqslant 1.0$) microparticles as active material by

using particle induced γ-ray emission (PIGE) and particle induced X-ray emission (PIXE), respectively. Li distribution maps of individual secondary particles (active material) are shown. The dependences of the Li distribution on electrode thickness as well as, on the charge process parameters are presented.

2. Experimental set-up

We have measured Li ion battery positive electrodes with thickness of 35 μm and 105 μm, which consist of $Li_xNi_{0.8}Co_{0.15}Al_{0.05}O_2$ ($0.75 \leqslant x \leqslant 1.0$) micrometer size particles as active material [10–12] mixed with artificial carbon and binder (note that no electrolyte in the sample), where the weight percentages are 85% for active material, 10% for carbon and 5% for binder. This positive electrode is coated on an Al current collector of 20 μm thick.

For fabricating charged samples, the above described positive electrode is attached to an electrolyte and a Li metal negative electrode for charging. Then, the current is applied. The specific charge conditions are summarized in Table I. After charge, the battery is quickly dissembled, typically within 3 min, and the liquid electrolyte is dried out to quench the Li-diffusion. In this way, the Li depth distribution after the charge is preserved. Then, the positive electrode was dissembled and cut to observe its cross section. It is worthwhile to mention that the drying process is intended not to substantially influence the Li distribution in the electrolyte. Thus, the Li distribution in the electrolyte prior to and after the drying process is assumed to be the same.

The Li and Ni spatial distributions are simultaneously characterized for as-received (prior to any charge cycle) and charged (under different conditions) positive electrode cross sections by μ-PIGE and μ-PIXE, respectively. PIGE measurements were carried out by using the $^7Li(p, p'\gamma)\ ^7Li$ nuclear reaction. Measurements were carried out at the microbeam line of TIARA-JAEA [13]. For the measurements a H^+ beam at an energy of 3.0 MeV was used. The beam current was selected to be 300 pA. The total accumulated charge per map was around 0.48 μC. The beam current was measured in a conductor foil located at the sample holder. The beam diameter, full width at half maximum, was 1.5 μm and the total scan areas were $\leqslant 200 \times 200\ \mu m^2$. The scanning step was 128 of the total scan range, providing 128×128 space points for each image. Measurements were carried out in high vacuum at a pressure range of 10^{-5} mbar in order to achieve a good beam spatial resolution. Nevertheless, because of the microbeam halo effects and the lateral straggling of the beam penetrating into the samples, the lateral resolution of the microbeam scans is somewhat larger than the beam diameter. The characteristic emitted γ- and X-rays were collected by a HPGe and by a Li-doped Si detector located at 0° and at 140° to the beam direction, respectively. Under these conditions, typical measuring times were around 30 min. We note that these experimental conditions avoid beam-induced lithium diffusion. Indeed, several spectra were sequentially measured on the same measuring area up to a dose of three times higher than that used in real experiments and no ion beam-induced lithium diffusion was detected. The data acquisition system uses the Microsoft Visual BASIC and runs on the Windows-based PC platform.

For measuring the cross sectional distributions of Li in the electrodes, the electrode cross sections were polished for 10 h by using a focused Ar beam at an energy of 6 keV prior to the ion beam analysis. The beam current of the JEOL SM-09010 Cross Section Polisher was 120 μA. Special precautions were taken during the cutting process to prevent the diffusion of light elements, in particular Li. Indeed in order to be sure that the cutting process does not influence the Li distribution, measurements are carried out for the samples cut from two opposite directions. No significant difference between them was observed. The morphology of the electrode was characterized by means of electron scanning microscopy (SEM) using a HITACHI S-4300 microscope.

3. Results and discussion

A brief overview of the studied samples together with the charge conditions is listed in Table I.

3.1. Elemental composition characterization

The elemental distribution is characterized by μ-PIGE and μ-PIXE techniques. Typical μ-PIGE and μ-PIXE spectra for an as-received and a charged positive electrode are shown in Fig. 1a and b, respectively. The nuclear reactions which contribute to the observed gamma ray spectra are also shown in the table in Fig. 1. These data illustrate that the samples are composed of the active material elements: Ni, Co and Al. Some other elements such as F and O are binder constituents. As illustrated in Fig. 1a (inset), the Li yield is higher for the uncharged than for the charged electrode, whereas the Ni yield (Fig. 1b) is almost the same in both of them. From these data the Li/Ni ratio is estimated to be 1.10 for the as-received electrode and 0.94 for the charged one.

It is worthwhile to mention that according to TRIM Monte Carlo [14] simulations, the 3 MeV proton beam penetration depth is calculated to be 58 μm by assuming an electrode density of 2.1 g/cm^3. Thus, the resulting γ-ray yields are sums of yields from the sample surface up to the depth of 58 μm.

SEM images of the as-received electrode, depicted in Fig. 2a, show a high density of micro-particles randomly distributed at high density with arbitrary shapes and sizes ranging from 5 to 10 μm. μ-PIGE (Fig 2b) and μ-PIXE (Fig 2c) maps, estimated from the defined region of interests, reveal that the micro-particles contain Li, Ni, Co and Al (Co and Al maps are not shown). Thus, they are $Li_xNi_{0.8}Co_{0.15}Al_{0.05}O_2$ secondary particles. By comparing SEM, μ-PIGE and μ-PIXE images, complete correspondence between these images is deduced.

3.2. Li distribution within the secondary particle

One important parameter to be controlled in further development of Li-ion batteries is the homogeneity of the Li distribution within individual secondary particles. Previous works carried out on $LiCoO_2$, $LiNiO_2$ and $LiFePO_4$ evidence that these positive electrodes present two-phase transitions during Li intercalation and Li extraction, which give rise to an asymmetric Li distribution (Li-rich and Li-depleted regions) within the individual particles of active material [15]. This two-phase transition is very undesirable

Table I
Brief overview of sample codes, thickness and charge parameters for the analyzed electrodes.

Sample code	Thickness (μm)	Charge current density (mA/cm^2)	Charge time (min.)
SP1-20-0-0	20	0	0
SP2-20-0-0	20	0	0
SP3-20-0.005-6000	20	0.005	6000
SP4-20-0.005-6000	20	0.005	6000
PE105-6-15	105	6	15
PE35-2-15	35	2	15
PE105-0.6-150	105	0.6	150

*The sample code (SPX-T-D-t) corresponds to SP: individual secondary particle, X: particle number, T: sample thickness, D: charge current density, and t: charge time. The sample code (PE-T-D-t) corresponds to PE positive electrode, T: sample thickness, D: charge current density, and t: charge time.

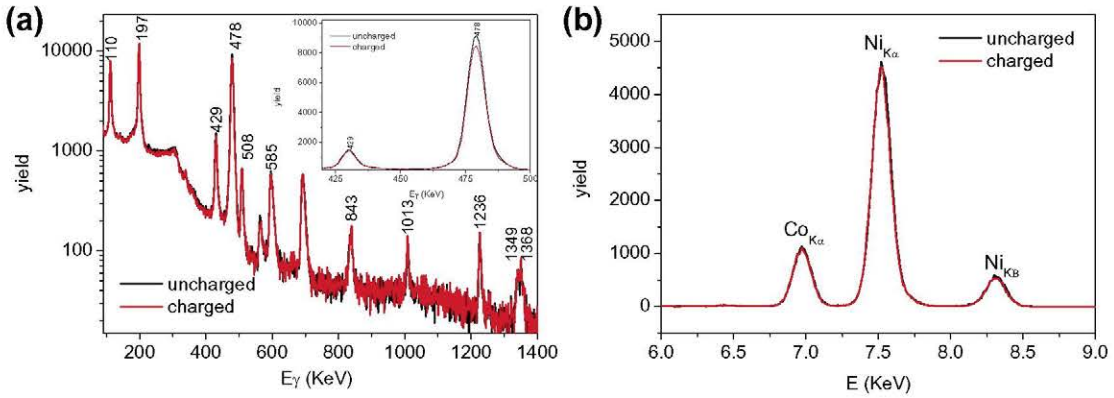

Eγ (keV)	Reactions
110	$^{19}F(p, p\gamma_{1\text{-}0})^{19}F$
197	$^{19}F(p, p\gamma_{2\text{-}0})^{19}F$
429	$^{7}Li(p, n\gamma_{1\text{-}0})^{7}Be$
478	$^{7}Li(p, p\gamma_{1\text{-}0})^{7}Li$
585	$^{25}Mg(p, p\gamma_{1\text{-}0})^{25}Mg$
843	$^{27}Al(p, p\gamma_{1\text{-}0})^{27}Al$
1013	$^{27}Al(p, p\gamma_{2\text{-}0})^{27}Al$
1236	$^{19}F(p, p\gamma_{3\text{-}1})^{19}F$
1349	$^{19}F(p, p\gamma_{4\text{-}1+5\text{--}2})^{19}F$
1368	$^{27}Al(p, \alpha\gamma_{1\text{-}0})^{24}Mg$

Fig. 1. PIGE (a) and PIXE (b) spectra for an as-received, uncharged, (black line) and a charged (red line) positive electrode. (For interpretation of the references to color in this figure legend, the reader is referred to the web version of this article.)

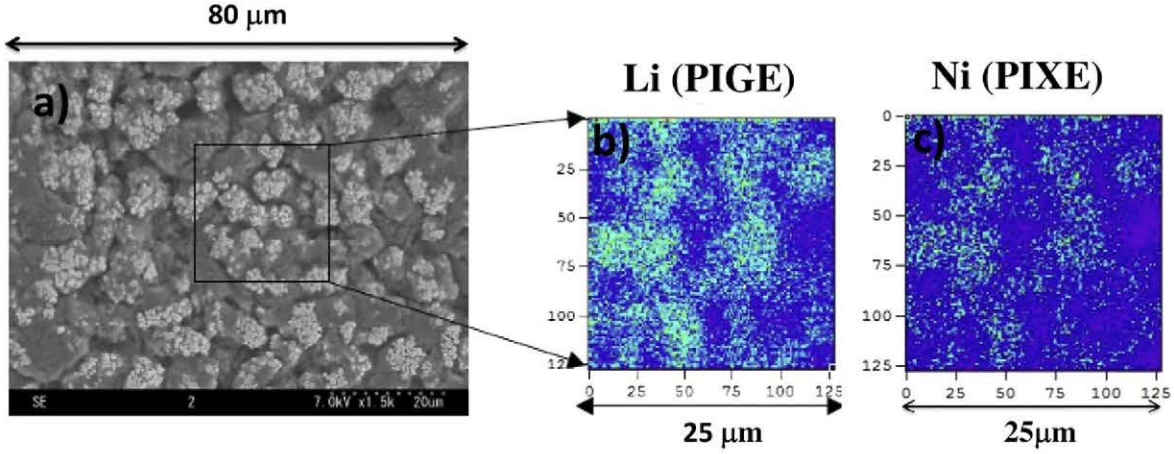

Fig. 2. SEM images (a) as well as, Ni (b) and Li (c) distribution maps for an as-received electrode. The size of the SEM image is 100 × 100 μm^2 and the size of the Li and Ni maps is 25 × 25 μm^2.

since it causes a long-term dependence between the internal resistance and the load history. Therefore, the in situ measurement of the Li distribution within the secondary particle is important.

In order to study the Li distribution within individual secondary particles, special samples consisting of isolated $Li_xNi_{0.8}Co_{0.15}Al_{0.05}O_2$ micro-particles were prepared. The SEM pictures and the Li and Ni distribution maps for two representative as-received samples are depicted in Fig. 3. It is important to note that neither smoothing nor imaging improvements tools were used to process the elemental distribution maps depicted in this publication. The Li/Ni ratio distribution (i.e. the fraction of Li relative to Ni) is calculated by dividing the Li signal with the Ni signal. The Li/Ni distributions shown in Fig. 3 are observed to be constant along the whole measured area, indicating that Li ions are homogeneously distributed

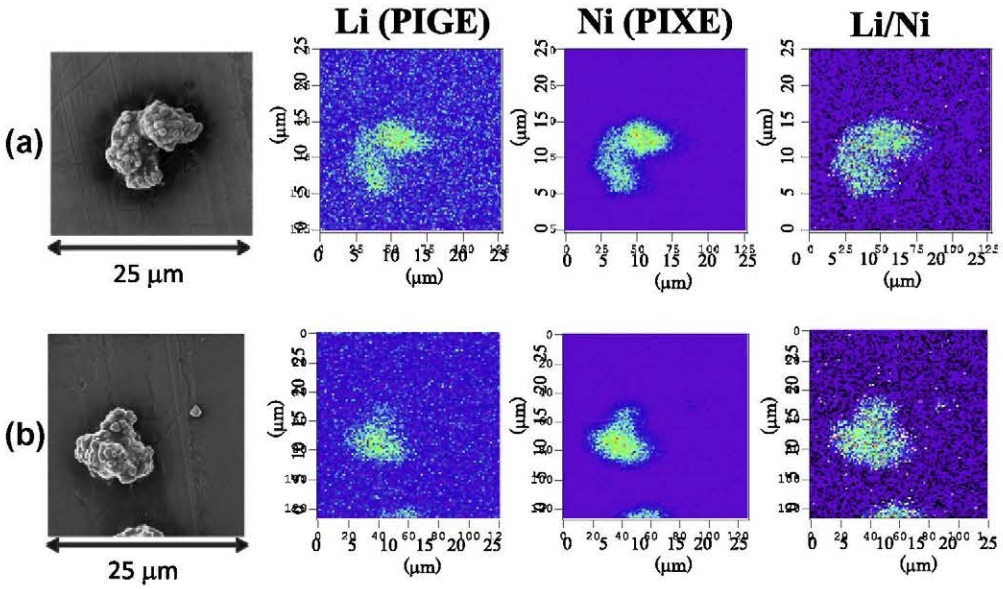

Fig. 3. SEM images, Ni and Li distribution maps and calculated Li/Ni ratio maps for two representative individual $Li_1Ni_{0.8}Co_{0.15}Al_{0.05}O_2$ microparticles. (a) SP1-20-0-0 and (b) SP2-20-0-0. The dimensions of the Ni and Li distribution maps are 25 × 25 µm^2.

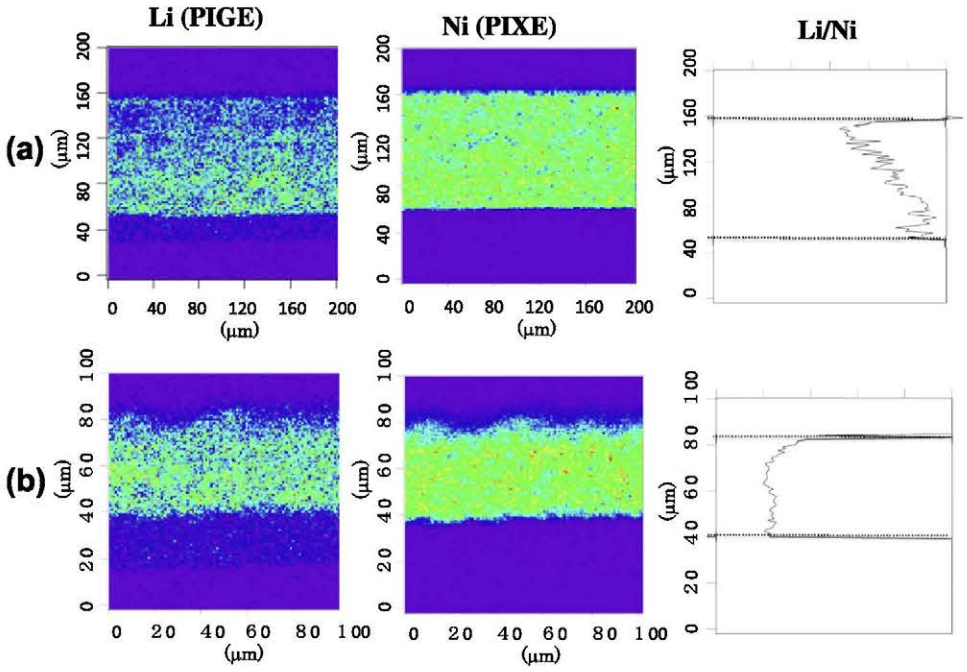

Fig. 4. Li and Ni distribution maps as well, as calculated Li/Ni ratio for two positive electrodes with different thickness both charged at the same rate: (a) PE35-2-15, and (b) PE105-6-15. The dimensions of the maps are 200 × 200 µm^2 and 100 × 100 µm^2.

in the studied secondary particles within our lateral resolution limit.

Further improvement of the measurement and charging procedure has to be carried out in order to characterize the Li distribution in charged individual micro-particles.

3.3. Electrode thickness dependence of the Li distribution

It has been reported that the electrode thickness notably influences the charge/discharge rate capability, energy density, power density and long-term cycling behavior of the Li-ion batteries [16]. Even though the electrode thickness is an important design parameter, its effect on battery performance has not been sufficiently investigated. In particular, as far as we know, the electrode thickness dependence of the overall Li distribution has not been characterized for several tens of µm thick samples.

In order to study the influence of the electrode thickness on the Li distribution, Li and Ni distribution maps are simultaneously measured for two charged positive electrodes with different thickness (35 µm for PE35-2-15 and 105 µm for PE105-6-15) both charged at the same rate per thickness, namely charged at 2 mA/cm^2 for PE35-2-15 and 6 mA/cm^2 for PE105-6-15 (see Table 1). The results for the 105 µm and for 35 µm thick electrodes are shown in Fig. 4(a and b), respectively. The separator is on the upper

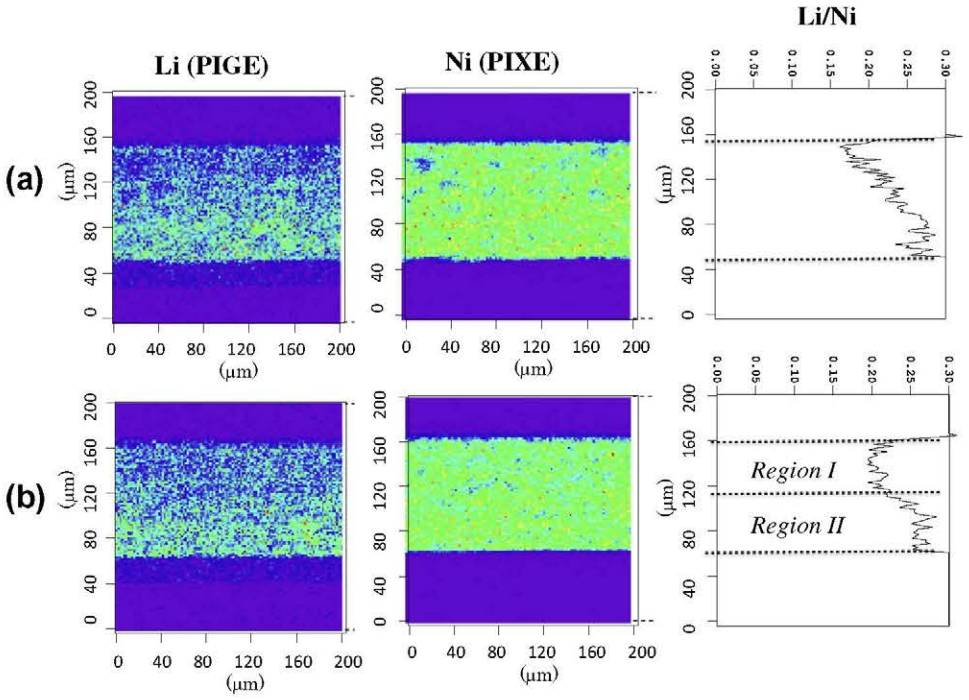

Fig. 5. Li and Ni distribution maps as well, as calculated Li/Ni ratio for two positive electrodes with a thickness of 105 μm charged under different conditions. (a) PE105-6-15, and (b) PE105-0.6–150. The dimensions of the maps are 200 × 200 μm^2.

side and the Al current collector in the lower side in these figures. From the uniform color distribution of the Ni signals in both data, we find that Ni is homogeneously distributed in these electrodes.

On the other hand, an inhomogeneous Li distribution is observed for the 105 μm thick electrode (Fig. 4a). Particularly, the Li content close to the Al current collector ($d \leqslant 30$ μm) is higher than at larger distances. This result is quantitatively presented by the Li/Ni ratio, which was calculated by integrating both signals along x for the same depth and then dividing the obtained values. The plot in Fig. 4(a) shows monotonous increase in the Li/Ni ratio from the separator side to the Al side. In contrast, very different situation is observed for the electrode with a thickness of 35 μm, where the Li distribution is almost constant along the whole thickness (Fig. 4b). These results point out that Li distributes more homogeneously in the thin electrode than in the thick electrode, showing the possibility of leading to better battery performances by selecting thin electrodes.

3.4. Li distribution dependence on the charge conditions

According to the literature [17], when the Li atoms are de-intercalated from the $Li_xNi_{0.8}Co_{0.15}Al_{0.05}O_2$ during the charge process, the Li concentration in the positive electrode is expected to be inhomogeneous. This inhomogeneity depends not only on the electrode thickness, but also on the charge rate, the electrode elemental composition and its structure. Here we have studied the influence of the charge rate on the Li distribution by measuring the Li and Ni maps for the two electrodes with a thickness of 105 μm which were charged under different conditions, 6 mA/cm^2 and 0.6 mA/cm^2, (PE1056-15 and PE105-0.6-150, see Table I). Charge parameters (current density and time) are selected in order to obtain the same charge state in both samples. The Li and Ni distribution maps are depicted in Fig. 5(a) for the fast charge electrode and in Fig. 5(b) for the slow charge. No color contrast is observed in the characterized Ni maps, indicating that, as expected, Ni is homogeneously distributed in the electrodes. The color contrast measured in the Li maps for both samples reveal that the Li ions inhomogeneously distribute for both electrodes. Moreover, significant differences are observed in the maps for the samples charged under different conditions. These differences become clearer by calculating the Li/Ni ratio. For the fast charged sample (PE105-6-15) a homogenous gradient in the Li distribution along depth is observed. In particular the Li distribution linearly decreases with increasing the distance from the Al current collector. However, for the sample charged with lower current (0.6 mA/cm^2) and longer duration (2.5 h), two well defined regions with an almost constant Li content in each but with a clearly different Li content in between them is observed. In this sample, the Li distribution near to the Al current collector (*region I*) is around 10% higher than in the region close to the separator (*region II*). A quite abrupt transition is observed between one region and the other. It is a new finding form the performance point of view that the Li distribution is non-uniform even for the slow charge sample.

4. Conclusion

The μ-PIGE and μ-PIXE spectroscopy techniques are successfully applied to accurately measure the Li distribution in the Li-ion batteries. Moreover, the use of the proton μ-beam allows characterizing the Li distribution with a spatial (lateral) resolution in the μm range.

The μ-PIGE maps evidence that the Li ions inhomogeneously distribute in the positive electrode due to the random distribution of the $Li_1Ni_{0.8}Co_{0.15}Al_{0.05}O_2$ secondary particles which is observed in the SEM images. However, the Li distribution within the as-received individual $Li_1Ni_{0.8}Co_{0.15}Al_{0.05}O_2$ secondary particles turns out to be homogeneous.

The Li distribution in the cross sections of the electrodes is observed to depend on the electrode thickness and on the charge conditions. The Li distribution is measured to be homogeneous in a thin electrode of 35 μm thickness, whereas it becomes very inho-

mogeneous when increasing the thickness to 105 μm. For the thick electrode of 105 μm, slow charge rate gives rise to a small gradient of the Li distribution in the electrode regions close to the Al current collector, which is indicated to be more favorable from the performance point of view.

In conclusion, we have demonstrated that the μ-PIGE is a powerful tool for the diagnostics of the Li-ion batteries. These results are relevant for further development of advanced Li-ion batteries with improved performances.

Acknowledgements

The proton beam irradiation experiments are supported by the TIARA operation team and the authors sincerely thank to the team. One of the authors (K. Mima) appreciates the fruitful discussions and encouragement of Professor Z. Ogumi and Professor Y. Uchimoto of Kyoto University and Mr. M. Takimoto of Toyota Central R&D Labs., Inc, and Professor Hiroaki Nishimura (ILE, Osaka University). Authors thank to Prof. E. Minguez and Dr. Fernando Sordo for the fruitful discussion and their support of this work. This research is supported by the Strategic International Cooperative Program (PRI-PIBJP-2011-0810) under Japan Science and Technology Agency (JST) and Ministerio de Ciencia e Innovación (MICINN).

J. Newman, K.E. Thomas-Alyea, Electrochemical Systems, John Wiley & Sons, 2004.
Y.S. Meng, T. McGilvray, M. Yang, D. Gostovic, F. Wang, D. Zeng, Y. Zhu, J. Graetz, Electrochem. Soc. Interface Fall (2011) 49–53.
L.B. Ellis, K.T. Lee, L.F. Nazar, Chem. Mater. 22 (2010) 691–714.
J.R. Wilson, J.S. Cronin, S.A. Barnett, S.J. Harris, J. Power Sources 196 (2011) 3443–3447.
I. Nakai, K. Takahash, Y. Shiraishi, T. Nakagome, J. Phys. IV France 7 (1997). C2-1243–C2-1244.
T. Nonaka, C. Okuda, Y. Ukyo, T. Okamoto, J. Synchrotron Rad. 8 (2001) 869–871.
J.R. Tesmer, M. Nastasi, Handbook of Modern Ion Beam Materials Analysis, MRS, Pittsburgh, PA, 1995.
T. Tadic, M. Jaksic, C. Capiglia, Y. Saito, P. Mustarelli, Nucl. Instr. Meth. Phys. Res. B 161-163 (2000) 614–618.
T. Tadic, M. Jaksic, Z. Medunic, E. Quartarone, P. Mustarelli, Nucl. Instr. Meth. Phys. Res. B 181 (2001) 404–407.
Y. Ito, Y. Ukyo, J. Power Sci. 146 (2005) 39–44.
T. Sasaki, Y. Ukyo, Etal, J. Electrochem. Soc. (2009) A289–A293.
S. Muto, Y. Ukyo, et al., J. Electrochem. Soc. (2009) A371–A377.
T. Sakai, T. Kamiya, M. Oikawa, T. Sato, A. Tanaka, K. Ishii, Int. J. PIXE 10 (2000) 91.
J.F. Ziegler, M.D. Ziegler, J.P. Biersack, SRIM-2006.02.
M.A. Roschera, J. Vetter, D.U. Sauer, J. Power Sources 191 (2009) 582–590.
H. Zhenga, J. Li, X. Song, G. Liu, V.S. Battaglia, Electrochim. Acta 71 (2012) 258–265.
Chemical Engineering Division, Argonne National Laboratory. Available from: http://www.osti.gov/bridge.